

Tensile strengths of hydrous vesicular glasses: An experimental study

C. ROMANO, J.E. MUNGALL, T. SHARP, AND D.B. DINGWELL

Bayerisches Geoinstitut, Universität Bayreuth, D-95440 Bayreuth, Germany

ABSTRACT

We have measured the pressures of decrepitation of vesicles in synthetic glasses of feldspar compositions ($\text{NaAlSi}_3\text{O}_8$ - KAlSi_3O_8). Vesicles filled with Xe do not decrepitate at internal pressures of 160 MPa, indicating that the unflawed surface of the vesicle wall has an intrinsic strength >80 MPa. Vesicles containing CO_2 escaped decrepitation and displayed ductile deformation when the T_g was reached at the maximum P of 200 MPa (indicating an intrinsic strength higher than 100 MPa). Vesicles containing H_2O showed dramatically reduced strength, decrepitating at internal pressures on the order of 1–5 MPa. The H_2O -filled vesicles leaked slowly over periods of several weeks or months. The relative stability of the inclusions is strongly dependent on the quench rate, with rapidly quenched inclusions showing greater stability over long periods of time. Microscopic examination revealed the presence of radial microfractures in the walls of H_2O -filled vesicles. We account for the microfracturing with reference to recent studies of chemical-gradient stress. Our observations may account for a variety of phenomena, which occur wherever hydrous vesicular glasses are formed, including explosive decompression of vesicular glassy rock in near-surface volcanic environments, spontaneous decrepitation of vesicular basaltic glass dredged from the seafloor (“popping rocks”), and rapid loss of H_2O from synthetic vesicular glasses produced in laboratory experiments investigating fluid-melt phase equilibria.

INTRODUCTION

The strength and physical integrity of vesicular glasses are properties of great importance in a variety of fields. Quantitative modeling of many volcanic processes requires a knowledge of the strength of glass surrounding vesicles (e.g., Sato et al. 1992); workers seeking to characterize volatiles trapped within vesicular glasses need to know how well vesicle-filling gases preserve their primary compositions (Paillat et al. 1992; Pineau and Javoy 1994). We measured the tensile strength of glass by fluid-inclusion techniques. Vesicles synthesized with CO_2 or Xe vapor allow determinations of tensile strength of ~ 100 MPa or more, which agree with previously published results (e.g., Webb and Dingwell 1990). However, in the presence of H_2O , the effective strength of vesicle walls is reduced up to two orders of magnitude, which we attributed to the generation of microfractures during dehydration of the glass-forming melt adjacent to cooling vesicles. The existence of microfractures may account for observed low strengths of some glassy volcanic materials, including “popping rock” dredged from the midocean ridges, and shallow intrusions of magma implicated in frequent explosive outbursts from choked vents.

EXPERIMENTAL METHODS

Glasses with compositions on the join albite-orthoclase were synthesized from oxide and carbonate powders in a

1 atm furnace in platinum crucibles and stirred with a platinum spindle to ensure homogeneity. The composition of the starting glasses was determined by ICP-AES. The results of the analyses are given in Table 1 as the proportions (weight percent) of the oxides. Powdered glass was loaded into platinum-metal capsules along with sufficient double-distilled H_2O , $\text{Ag}_2\text{C}_2\text{O}_4$, or Xe gas to ensure volatile oversaturation.

For the H_2O -solubility experiments, the amount of added H_2O was chosen to be about 3–4% higher than the expected solubility value (Romano et al. 1996). This value was high enough to prevent significant dilution by air enclosed in the capsule during preparation but low enough to minimize possible changes in the anhydrous stoichiometry of the melt resulting from incongruent dissolution of melt components in the H_2O fluid. The capsules were checked for possible leakage by testing for weight loss after drying in an oven at 100 °C for at least 1 h. After an hour at 100 °C, the volatile was considered to be distributed randomly (space filling) in the platinum capsule and thus around the glass sample. The H_2O -bearing samples were placed in cold-seal pressure vessels (H_2O as pressure medium), pressurized to 2 kbar, heated to 850 °C, and held at these conditions for sufficient time to allow vapor-melt equilibration by diffusion of the volatile constituents through the melt (experimental durations ranged from 3 to 5 d). Temperature was measured with an Ni-NiCr thermocouple (accuracy ± 15 °C). Pressure

TABLE 1. Analyzed anhydrous compositions (wt% oxide)

Glass	SiO ₂ (±0.6)	Al ₂ O ₃ (±0.4)	Na ₂ O (±0.5)	K ₂ O (±0.5)	Total	H ₂ O* (±0.1)
Na ₁₀₀	68.1**	19.1	11.8		99.0	6.03
Na ₉₀ K ₁₀	69.1	19.0	10.9	1.8	101.0	6.01
Na ₇₀ K ₃₀	67.8	19.0	8.0	5.4	100.2	5.94
Na ₅₀ K ₅₀	67.6	18.9	5.6	8.7	100.8	5.68
Na ₃₀ K ₇₀	66.4	18.8	3.3	12.0	100.5	5.51
Na ₁₀ K ₉₀	65.3	18.8	1.2	15.6	100.9	5.27
K ₁₀₀	65.4	18.5		16.5	100.4	5.12

Note: Na₁₀₀ = NaAlSi₃O₈ (albite), K₁₀₀ = KAlSi₃O₈ (orthoclase). Numbers in parentheses represent relative errors.

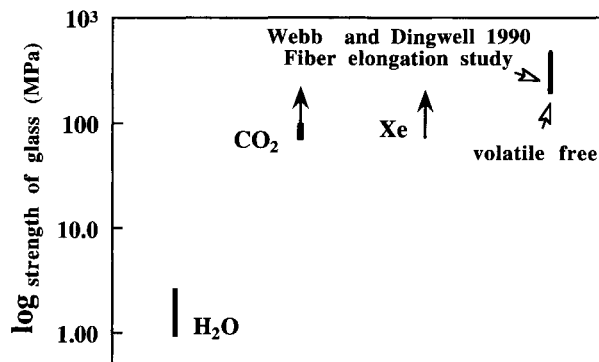
* Total H₂O content determined by Karl-Fischer titration (from Romano et al. 1996).

** Compositions determined by ICP-AES analysis.

quoted is accurate to ±0.02 kbar. CO₂-bearing samples were placed in TZM (titanium, zirconium, and molybdenum) and pressurized at 2 kbar and *T* = 1040 °C. Some CO₂ samples were also synthesized at *P* = 2 kbar and *T* = 850 °C in cold-seal pressure vessels. Xe-bearing samples were synthesized in TZM vessels (argon as pressure medium) at *P* = 2 kbar and *T* = 1040 °C. Temperature in the TZM vessels was measured with an Ni-NiCr thermocouple (accuracy ±15 °C), and the pressure was measured with a strain-gauge manometer (accuracy 0.05 kbar). After the high-pressure-high-temperature dwells, the samples were quenched isobarically in the vessels either by dropping the sample into the cold part of the vessels (estimated quench rate 200 °C/s) or by air quench (quench rate 200 °C/min). Special care was given during the quench to maintain isobaric conditions by opening the vessels to the pressure line. Total H₂O solubilities for the experimental conditions are presented in Table 1.

The H₂O contents of the feldspathic glasses range from 5.12 to 6.03 wt% (Romano et al. 1996). For comparison, CO₂ solubilities vary from approximately 1170 ppm (*P* = 2 kbar, *T* = 1100 °C) to 2200 ppm (*P* = 2 kbar, *T* = 850 °C) (Fogel and Rutherford 1990). Xe dissolves in rhyolitic melts up to about 250 ppm for the pressure of synthesis (value calculated from ionic porosity data from Carroll and Webster 1994).

The products of the experiments are vesicular glasses typically containing 20–40 vol% of approximately spherical vesicles ranging in size from 10 to 200 μm. The aspect ratios of the vesicles range between 1.0 and 1.4 for H₂O-bearing samples and from 1.0 to 1.1 for Xe and CO₂-bearing samples. Application of standard fluid-inclusion methodology permits the identification of the included volatiles and of the trapping temperature (Romano et al. 1994). The volatiles present in the vesicles were identified by measurement of homogenization and freezing temperatures, which confirm that they consist either of pure H₂O, CO₂, or Xe. Heating of vesicular glass in a fluid-inclusion heating stage generates a controlled internal pressure, because below the glass-transition temperature the vesicle dimensions remain essentially constant (thermal expansion of the glass is negligible) and the



Volatile

fluid is thus constrained to constant volume (Romano et al. 1994). The tensile tangential stress $\sigma_{\theta\theta}$ generated in the wall of a spherical vesicle as a result of differences between internal pressure P_1 and external pressure P_2 is (Landau and Lifshitz 1987)

$$\sigma_{\theta\theta} = \frac{P_1 b^3 - P_2 a^3}{a^3 - b^3} + \frac{(P_1 - P_2)}{2r^3 \left(\frac{1}{b^3} - \frac{1}{a^3} \right)} \quad (1)$$

where a is the outer shell, b is the outer diameter of the vesicle, and r is the radial space coordinate. When a is equal to infinity ($a = \infty$) and $r = b$ then the equation becomes

$$\sigma_{\theta\theta} = \frac{P_1 - 3P_2}{2} \quad (2)$$

During reheating of the samples, $P_2 \approx 0$, so that $\sigma_{\theta\theta} = P_1/2$. The strength of the glass is therefore directly measured by the internal pressure of the vesicles at the time of decrepitation. In vesicles with nonspherical shapes, the regions of the walls with the smallest radius of curvature concentrate stress, resulting in failure at lower pressures (cf. Ernsberger 1969); however, for aspect ratios <1.5 this effect adds uncertainty to our measurement of less than a factor of two.

RESULTS AND DISCUSSION

The strengths of vesicle walls as determined from decrepitation experiments are shown in Figure 1. The systems containing different volatiles show very different behavior. The samples containing pure Xe-filled inclusions did not decrepitate at 160 MPa, the upper limit of the pressure attainable in the vesicles during heating in the microthermometric stage (*T* = 600 °C). A few anomalous

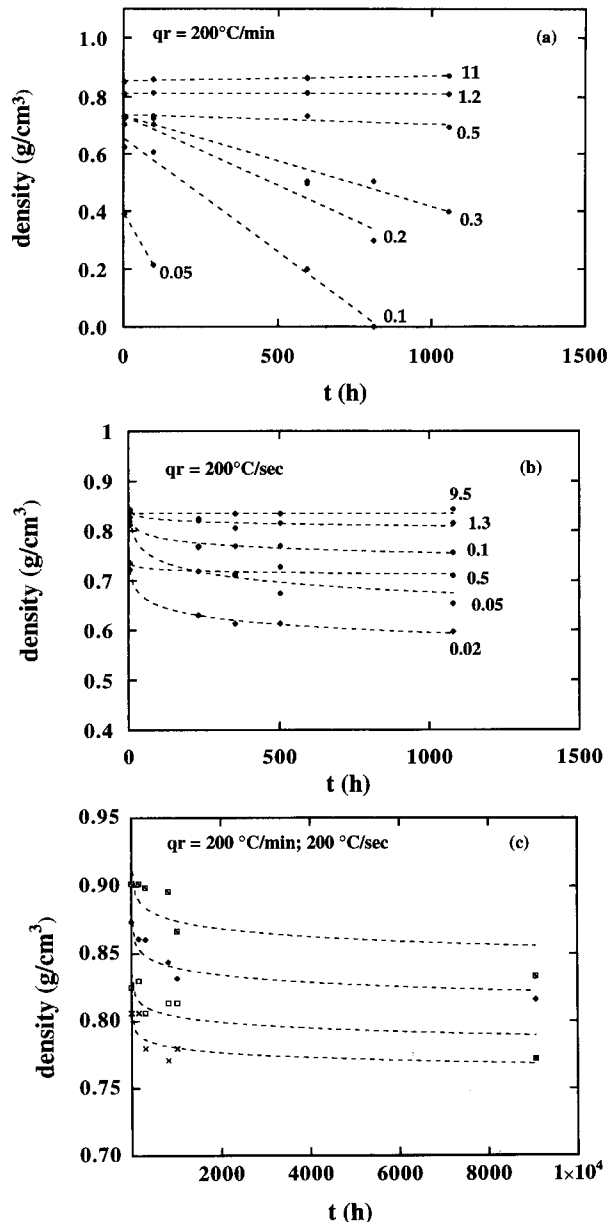


FIGURE 2. Stability of vesicles at room temperature and change in net fluid density within vesicles measured as a function of time. The change in density was measured by the volume change of the vapor bubble with time in inclusions chosen from various samples. The slow-quench samples (a) are compared with the samples quenched rapidly (b) for some representative inclusions. The volume of the vesicles is also shown ($\times 10^6 \mu\text{m}^3$). The time $t = 0$ of the first density determination is ≈ 5 h after quenching (see text). Rapid fluid loss is favored both by smaller inclusion size and by slower quench. (c) Change in fluid density after 1 yr of observation for both slowly and rapidly quenched samples. Inclusions larger than a critical size of $\sim 50 \mu\text{m}$ stopped leaking before becoming completely empty. This suggests that the fluid escapes into a zone of constant width surrounding vesicles of different sizes.

CO_2 -bearing inclusions decrepitated at internal pressures between 150 and 200 MPa (maybe indicating variations in aspect ratio); however, the great majority of the inclusions escaped decrepitation altogether and instead displayed ductile stretching deformation when the glass-transition temperature was reached at the maximum pressure of 200 MPa. The presence of crystals in some of the experimental products as well as variations in the composition of the glass along the alkali feldspar join and variation in the temperature of synthesis did not have any measurable effects on the decrepitation behavior (e.g., Ernsberger 1969). The decrepitation behavior of the H_2O -bearing inclusions was radically different from that of the other two types. At internal pressures of < 1.5 MPa all vesicles were seen to lose fluid rapidly without any change in dimensions; at pressures above 1.5 MPa vesicles started decrepitating, and at pressures above 5 MPa all vesicles in the sample decrepitated. The extensive fracturing that resulted reduced the glass to fine particles. The effective strength of the walls around pure- H_2O -bearing vesicles was therefore between 0.75 and 2.5 MPa.

The very rapid loss of fluid from H_2O -bearing vesicles observed in the heating experiments was complemented by similar longer-term behavior at room temperature. The relationship between net fluid contents of inclusions (expressed as fluid density) and the dimensions of the vesicles is shown in Figure 2. The initial density ρ_i of the fluid is obtained as

$$\rho_i = \frac{(V_{\text{incl}} - V_{\text{vap}})}{V_{\text{incl}}} \quad (3)$$

where V_{vap} is the volume expressed in cubic micrometers of the vapor phase inside the inclusions and V_{incl} is the total volume of the vesicle (assuming that the density of the liquid phase is ~ 1 and that the vapor is ~ 0 at 25°C).

The initial densities ($t = t_0$) are different in different vesicles because the rate of fluid loss varies exponentially with time and is highest immediately after quenching. The different densities correspond to a fluid loss that occurs between the end of the experiment and the initial optical determination of the density of the sample (a few hours). This early loss of H_2O leads to lower density (larger loss) for small inclusions and higher density (minor loss) for large inclusions. The t_0 density (i.e., density under trapping conditions of $P = 2$ kbar and $T = T_g$) is very close to the density measured for large inclusions (0.85–0.90 g/cm^3), for which the fluid loss with time can be considered negligible. Vesicle density is initially a linear function of time in all cases and drops more rapidly in smaller vesicles. Vesicles in samples quenched rapidly from the conditions of synthesis (200°C/s ; Fig. 2b) leaked much more slowly than those in samples quenched slowly (200°C/min ; Fig. 2a). Slowly quenched vesicles with a diameter smaller than a critical value ($\sim 50 \mu\text{m}$) eventually lost all fluid. However, observation of vesicle densities over a 1 yr period revealed that many of the inclusions characterized by relatively slow rates of leakage, regardless of the quench rate of synthesis, stopped leaking

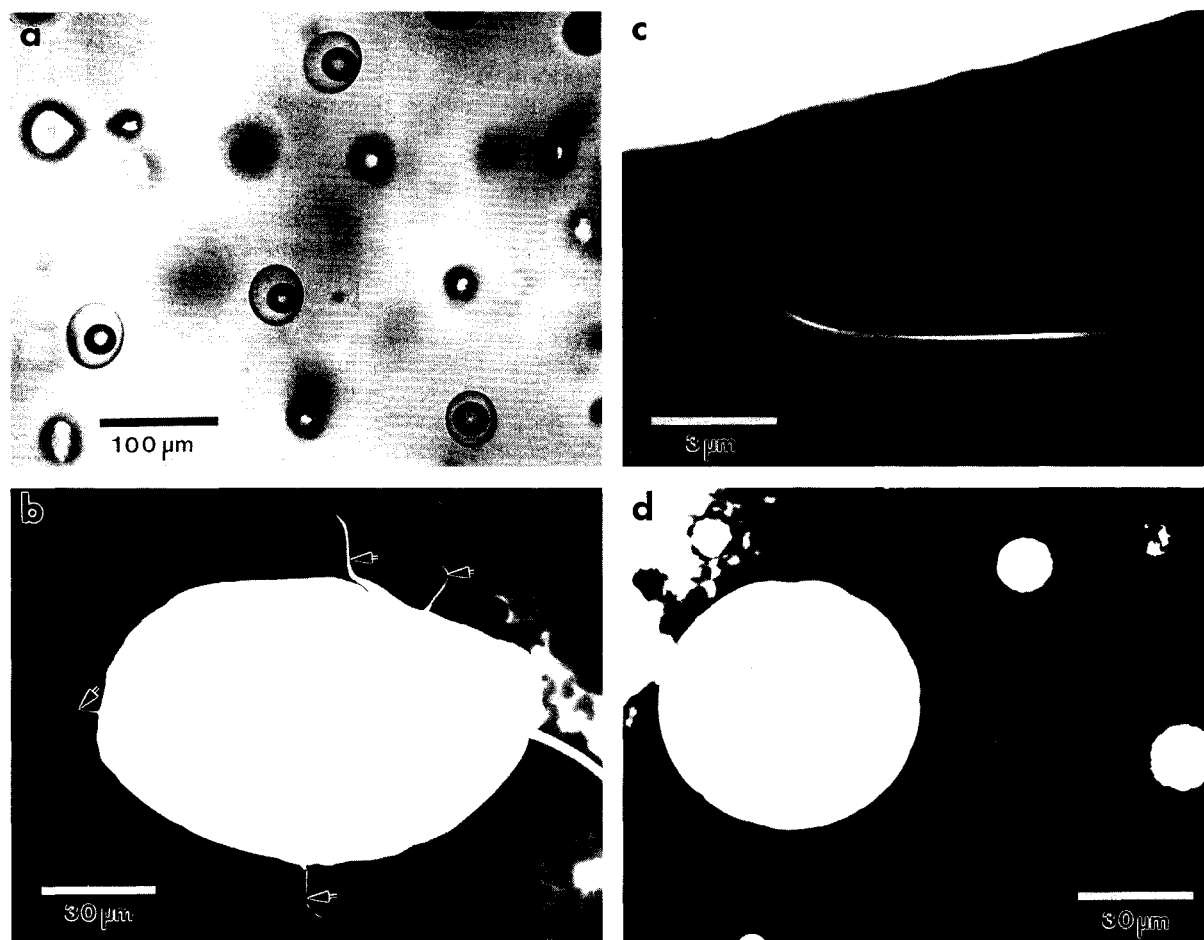


FIGURE 3. TEM images. (a) H₂O-bearing fluid inclusions in a glass of albitic composition. (b) Microfractures around an H₂O-filled vesicle. It was apparent on textural grounds that the fractures had been forced open somewhat during sample preparation, so that observed widths between 10 and 1000 nm must be

considered upper limits of the original dimensions. (c) The deflection of the microfracture from a radial to a tangential orientation may reflect the change from tensile to compressive stress in the tangential stress component predicted by modeling (Mungall et al. 1996). (d) CO₂-bearing vesicle with no microfractures.

before becoming completely empty (Fig. 2c). These observations are consistent with fluid loss to a reservoir of limited capacity consisting of a localized array of microfractures surrounding each vesicle. The reservoir associated with rapidly quenched samples is much smaller than that of slowly quenched samples, leading to better retention of fluid content but not greater tensile strength.

A TEM image of H₂O-bearing inclusions in a glass of albitic composition is shown in Figure 3a, illustrating typical vesicle distributions and spacings among the inclusions. TEM examination of the formerly H₂O-filled vesicles in cryogenically ion-thinned samples revealed the presence of numerous microfractures several tens of micrometers long and <1 μm wide (Figs. 3b and 3c). Microfractures were not observed in CO₂- and Xe-bearing samples (Fig. 3d). The combination of extremely low effective tensile strength, leakage, and microscopic obser-

vations of the walls of H₂O-bearing vesicles indicates unequivocally that these vesicle walls are flawed by the presence of microfractures. It is unlikely that the fractures are artifacts induced by sample preparation, because they appear only in samples characterized by anomalously low tensile strength and long-term vesicle leakage. Slow, subcritical growth of the microfractures over extended periods can account for the observed long-term fluid loss, whereas decrepitation of these vesicles upon reheating is consistent with a transition from subcritical to unsteady crack growth at a critical pressure of ~5 MPa (Lawn 1993, p. 86).

We propose that the microfractures observed in the H₂O-rich experiments were caused by contraction of the glass surrounding the vesicles during quench of the samples. We have described elsewhere in detail the evolution of stress surrounding vesicles in cooling vesicular glasses

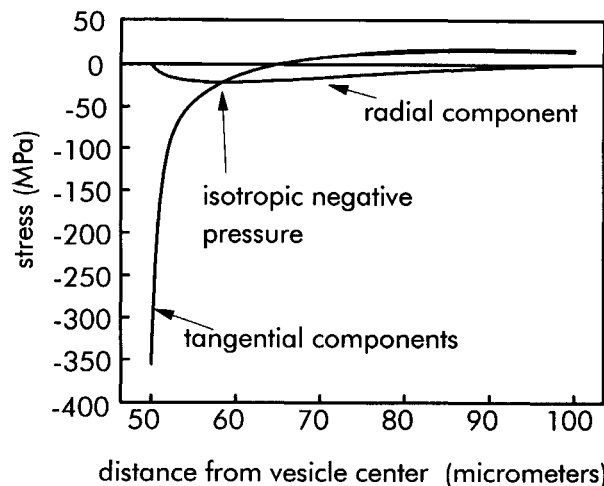


FIGURE 4. Distribution of stress around a vesicle with a radius of about 50 μm at the time of microfracture initiation. Owing to the diffusion of H_2O , the tangential stress component is tensile close to the vesicle wall but decreases rapidly with distance from the vesicle. When it is subequal to the radial stress component (also tensile), a negative pressure of about 20 MPa is exerted on the glass. The calculations were performed using the numerical model presented by Mungall et al. (1996), assuming 1.33 wt% initial H_2O content in the glass and a cooling rate of 10^{-3} K/s.

(Mungall et al. 1996); the salient points of that study are reiterated here. As the melt-vapor system is cooled above the glass-transition temperature the dimensions of vesicles adjust to the change in molar volume of the volatile phase by viscous relaxation. However, after the melt is cooled below T_g the vesicle dimensions become fixed and the vapor is forced to cool isochorically, leading to a reduction in pressure. Such behavior is familiar to users of fluid-inclusion techniques. The solubility of H_2O in the glass shows only a slight dependence on the temperature, whereas the drop in pressure in the vesicle causes the chemical potential of H_2O in the vesicle to fall out of equilibrium with the H_2O dissolved in the glass. The result is a flux of H_2O from the glass into the vesicle. Because the density of dry glass is greater than that of hydrous glass, the dehydrating glass shrinks, causing a radial strain, which imposes tangential stresses on the vesicle wall. The tangential stresses are a cumbersome function of the distribution of H_2O and the geometry of the system. However, for a spherical vesicle completely isolated from the effects of other vesicles, in the limit of infinitely fast quench rate, the tangential stresses $\sigma_{\theta\theta}$ resulting from dehydration are given by the following expression adapted from Mungall et al. (1996):

$$\sigma_{\theta\theta} = \frac{E\Delta C}{(1-\nu)} \quad (4)$$

where $\sigma_{\theta\theta}$ and ν are Young's modulus (5.08×10^{10} Pa) and Poisson's ratio (0.18) of the glass (Bagdassarov et al. 1993) and ΔC is the change in H_2O content in weight percent. We found that a change in H_2O content of 0.58

wt% is sufficient to induce tensile stresses of 350 MPa, the value we adopted as the approximate tensile strength of glass (Webb and Dingwell 1990). It therefore appears that any vesicular glass containing more than approximately 0.58 wt% H_2O should display microfractures around vesicle walls and a consequent weak response to overpressure in the vesicles.

In our hydrous experiments the change in H_2O content in the vesicle walls as the internal pressure in the vesicle changed from 200 to <0.1 MPa was 6 wt%, leading us to infer the existence of microfractures in all our samples.

The maximum tangential stress is tensile and occurs at the vesicle wall (glass-fluid interface) (Fig. 4). This stress component drops very rapidly with increasing radius and is equal to the radial stress component within several micrometers of the vesicle wall. A fracture initiated in the vesicle wall would propagate radially as long as the least principle stress is tangential. In the region of isotropic stress, where the three stress components are subequal, the fracture might either stop advancing or pass through into the region where the principal tensile stress is radial, leading to its deflection into a concentric shell. The latter pattern was observed in our experimental products (Fig. 3).

Effect of quench rate and vesicle size

Quenching in all our experiments was sufficiently rapid to ensure that the diffusive boundary layers surrounding vesicles did not interact to any significant degree. The experiments quenched more rapidly are expected to show exceedingly narrow boundary layers, ~ 100 nm, whereas the slowly quenched samples should show boundary-layer widths of ~ 5 – 10 μm (Mungall et al. 1996). Although in both cases we anticipated the generation of microfractures during quench, it is obvious that in the rapidly quenched samples the total volume of the region affected by dehydration and microfracturing is negligible in comparison with the volume of all but the smallest vesicles. In contrast to this, the volume of the disturbed region surrounding the slowly quenched vesicles is on the same order as that of the vesicles themselves. We suggest that the different behaviors of the two groups of samples can be accounted for by the relative sizes of the disturbed volumes surrounding the vesicles. The predicted existence of microfractures in both slowly and rapidly quenched samples is consistent with the observed low strengths of both groups, whereas the tendency for the contents of slowly quenched vesicles to drain away over long periods of time is consistent with the prediction that a relatively large volume of glass surrounding each vesicle would be disturbed during quenching.

The dependence of H_2O -loss rate on vesicle size (Fig. 2) can be accounted for by the same reasoning. More rapid and extensive H_2O loss is expected from smaller vesicles because the relative volume of the disturbed region is much greater in these cases. We observed that inclusions larger than a critical size, ~ 50 μm , displayed negligible variation in density over a period of >1 yr.

The exact cause of the H_2O loss is not entirely clear,

and we propose two possible mechanisms. One is simply slow, steady crack propagation over periods of days to months, leading to drainage of fluid into the cracks. It is not clear whether the observed volume of cracks could hold all the H₂O that was seen to depart from the vesicles. A second, more speculative suggestion, relates to the observation that there exists in the glass surrounding each vesicle a region of negative pressure, where all three stress components are tensile. Interactions between stress fields and other thermodynamic parameters are known to occur (Larche and Cahn 1982), however we are not aware of any published work describing the effects of negative (tensile) pressures on H₂O solubility in glass. Because dehydration of glass leads to negative dilatation (shrinkage), it might be reasonable to propose that the imposition of a positive dilatation could lead to radically enhanced H₂O solubility and transport rates, even at room temperature.

Direct observation of the microfractures (Fig. 3) is difficult and time consuming. Although we are able to make the qualitative observation that microfractures are common around the weak, H₂O-filled vesicles and absent around the strong, CO₂- and Xe-filled vesicles, we fear that artifacts induced during sample preparation (e.g., lengthening of fractures) would invalidate any attempt at quantitative interpretation of the TEM images. Because we cannot confidently relate fracture size or abundance to controlled parameters such as quench rate or vesicle size, we must leave the details of the mechanism controlling long-term H₂O loss an open question.

Effects of vesicle spacing

At the quench rates and vesicle spacings obtained in our experiments we neither anticipated nor observed any effects relating to the distances between vesicles, because these distances greatly exceed the maximum estimated width of a diffusive boundary layer of approximately 10 μm . At the much slower quench rates characteristic of the inner portions of cooling magma bodies some effects of vesicle spacing should be observed (Mungall et al. 1996). These effects can be understood qualitatively by considering Equation 4. If two vesicles are near enough to each other that their diffusive boundary layers begin to interact, the H₂O content of the glass between them diminishes, thereby reducing the parameter ΔC . In this way the stress is diminished; if either the quench rate is slow enough or the vesicles are close enough together to significantly reduce the residual H₂O content between the vesicles, then microfracturing is retarded or even suppressed altogether.

In our experiments, the confining pressure was maintained at 200 MPa until the samples cooled to room temperature, at which point their internal fluid pressures were considerably less than the atmospheric pressure of 0.1 MPa, constraining the fractures to remain confined to the local surroundings of the vesicles. If however, the confining pressure is released at any time during cooling above a critical temperature T , the residual vapor pressure in the vesicle is no longer opposed by an external force, and the glass itself then takes up the stress applied by the pore

vapor pressure. The existence of microfractures in the vesicle wall greatly lowers the bulk strength of the glass around the vesicle, and even very small drops in external pressures are sufficient to extend the microfractures outward until they intersect each other. Thus, the result of depressurization of the weakened glassy vesicular material may be sudden and spontaneous failure of vesicle walls, leading to disaggregation of the bulk material, possibly on a very short (explosive) timescale. We documented this behavior in our experiments. Below we consider some cases in which similar behavior is observed in nature and in other laboratory analogs.

Sudden release of comparatively small confining pressures of several megapascals is commonly observed to lead to small explosive eruptions from vent-filling plugs of lava such as the spine at Mount Pélée in 1902 and 1903 (Jaupart and Allègre 1991). Explosive rupture of vesicular rock at volatile overpressures nearly two orders of magnitude less than the tensile strength documented here requires the action of stress-concentrating flaws (Mungall 1995). The microfractures we have shown to exist are examples of such flaws.

Similarly, the spontaneous decrepitation of vesicular basaltic glass dredged from the ocean floor ("popping rock"; Pineau and Javoy 1994) occurs at volatile pressures much less than the known confining strength of the mafic glass, estimated to be about 250 MPa, somewhat less than that of felsic glasses (Webb and Dingwell 1990). The basaltic glass is known to contain about 0.5 wt% H₂O, so that microfractures would be expected to form during quench (Eq. 4). Because the quenched vesicles contain about 95 wt% CO₂, the vesicle contents at temperatures near 0 °C (the approximate temperature of deep-ocean H₂O) would include a CO₂-H₂O clathrate phase and would be below the liquid-vapor curve for CO₂, which is at about 3.5 MPa at $T = 0$ °C (e.g., Roedder 1984, p. 240). Warming of the sample to 20 °C on the ship's deck melts the clathrate phase and raises the internal pressure to 5.7 MPa on the liquid-vapor curve for CO₂. This pressure is still much less than the strength of pristine glass that we have measured in vesicles containing pure CO₂, but it is sufficient to decrepitate vesicles flawed by microfractures. These vesicles would have previously escaped decrepitation because of the presence of a hydrostatic confining pressure exerted by several kilometers of sea H₂O.

The observation that H₂O leaks from vesicles can have some bearing on the common observation that H₂O-rich glasses lose H₂O to the atmosphere at extraordinary rates (e.g., Paillat et al. 1992), many orders of magnitude greater than appear to be accounted for by chemical diffusion of H₂O through the glass (Zhang et al. 1991). In our experiments the microfractures produced a limited, isolated volume of pore space surrounding each vesicle. Because the microfractures are not interconnected, the observed leakage does not actually constitute a net loss of H₂O from the bulk sample. However, it is possible that in glasses with higher H₂O contents, showing prograde solubility or more closely spaced vesicles, the networks of

fractures become interconnected, permitting H₂O to escape to the surrounding atmosphere.

Finally, the observations of microfracturing of vesicle walls could have important implications for studies of natural or synthetic fluid inclusions in glasses (Romano et al. 1994, 1995). We have illustrated a phenomenon that greatly affects the stability of fluid inclusions both at room temperature and during heating in the microthermometric stage. We found that the relative stability of the inclusions is strongly dependent on the quench rate, with rapidly quenched inclusions showing greater stability over long periods of time. We therefore recommend that investigators synthesizing fluid inclusions seek to attain the highest possible cooling rates from their experimental conditions.

ACKNOWLEDGMENTS

We thank Anna Dietel for analytical assistance. This work has been supported by the Deutsche Forschungsgemeinschaft Gerhard-Hess-Programm (Di 431/3-1) and a Canadian Natural Science and Engineering Research Council Fellowship to J.E.M.

REFERENCES CITED

- Bagdassarov, N., Dingwell, D.B., and Webb, S. (1993) Effect of boron, phosphorus and fluorine on shear stress relaxation in haplogranitic melts. *European Journal of Mineralogy*, 5, 409–425.
- Carroll, M.R., and Webster, J.D. (1994) Solubilities of sulfur, noble gases, nitrogen, chlorine, and fluorine in magmas. In *Mineralogical Society of America Reviews in Mineralogy*, 30, 231–271.
- Ernsberger, F.M. (1969) Tensile and compressive strength of pristine glasses by an oblate bubble technique. *Physics and Chemistry of Glasses*, 10, 240–245.
- Fogel, R.A., and Rutherford, M.J. (1990) The solubility of carbon dioxide in rhyolitic melts: A quantitative FTIR study. *American Mineralogist*, 75, 1311–1326.
- Jaupart, C., and Allègre, C.J. (1991) Gas content, eruption rate and instabilities of eruption regime in silicic volcanoes. *Earth and Planetary Science Letters*, 102, 413–429.
- Landau, L.D., and Lifshitz, E.M. (1987) Theory of elasticity. In *Course of theoretical physics*, vol. 6 (2nd edition), 730 p. Pergamon, New York.
- Larche, F.C., and Cahn, J.W. (1982) The effect of self-stress on diffusion in solids. *Acta Metallurgica*, 30, 1835–1845.
- Lawn, B.R. (1993) Fracture of brittle solids (2nd edition), 378 p. Cambridge University Press, Cambridge, U.K.
- Mungall, J.E. (1995) Textural controls on explosivity of lava in Merapi-type block and ash flows. *Periodico di Mineralogia*, 64, 233–234.
- Mungall, J.E., Bagdassarov, N.S., Romano, C., and Dingwell, D.B. (1996) Numerical modelling of stress generation and microfracturing of vesicle walls in glassy rocks. *Journal of Volcanology and Geothermal Research*, in press.
- Paillat, O., Elphick, S.C., and Brown, W.L. (1992) The solubility of water in NaAlSi₃O₈ melts: A re-examination of Ab-H₂O phase relationships and critical behavior at high pressures. *Contributions to Mineralogy and Petrology*, 112, 490–500.
- Pineau, F., and Javoy, M. (1994) Strong degassing at ridge crests: The behavior of dissolved carbon and water in basalt glasses at 14°N, Mid-Atlantic Ridge. *Earth and Planetary Science Letters*, 123, 179–198.
- Roedder, E. (1984) Fluid inclusions. In *Mineralogical Society of America Reviews in Mineralogy*, 12, 644 p.
- Romano, C., Dingwell, D.B., and Sterner, S.M. (1994) Kinetics of quenching of hydrous feldspathic melts: Quantification using synthetic fluid inclusions. *American Mineralogist*, 79, 1125–1134.
- Romano, C., Dingwell, D.B., and Behrens, H. (1995) The temperature dependence of the speciation of water in NaAlSi₃O₈-KAlSi₃O₈ melts: An application of fictive temperatures derived from synthetic fluid inclusions. *Contributions to Mineralogy and Petrology*, 122, 1–10.
- Romano, C., Dingwell, D.B., Behrens, H., and Dolfi, D. (1996) Compositional dependence of H₂O solubility along the joins NaAlSi₃O₈-KAlSi₃O₈, NaAlSi₃O₈-LiAlSi₃O₈, and KAlSi₃O₈-LiAlSi₃O₈. *American Mineralogist*, 81, 452–461.
- Sato, H., Fujii, T., and Nakada, S. (1992) Crumbling of dacite dome lava and generation of pyroclastic flows at Unzen volcano. *Nature*, 360, 664–666.
- Webb, S.L., and Dingwell, D.B. (1990) The onset of non-Newtonian rheology of silicate melts: A fiber elongation study. *Physics and Chemistry of Minerals*, 17, 125–132.
- Zhang, Y., Stolper, E.M., and Wasserburg, G.J. (1991) Diffusion of water in rhyolite glasses. *Geochimica et Cosmochimica Acta*, 55, 441–456.

MANUSCRIPT RECEIVED JULY 3, 1995

MANUSCRIPT ACCEPTED MAY 6, 1996